

Influence of the Shape of Nanostructured Metal Surfaces on Adsorption of Single Peptide Molecules in Aqueous Solution

Jie Feng, Joseph M. Slocik, Mehmet Sarikaya, Rajesh R. Naik, Barry L. Farmer, and Hendrik Heinz*

Self-assembly and function of biologically modified metal nanostructures depend on surface-selective adsorption; however, the influence of the shape of metal surfaces on peptide adsorption mechanisms has been poorly understood. The adsorption of single peptide molecules in aqueous solution (Tyr_{12} , Ser_{12} , A3, Flg-Na₃) is investigated on even {111} surfaces, stepped surfaces, and a 2 nm cuboctahedral nanoparticle of gold using molecular dynamics simulation with the CHARMM-METAL force field. Strong and selective adsorption is found on even surfaces and the inner edges of stepped surfaces (-20 to -60 kcal/mol peptide) in contrast to weaker and less selective adsorption on small nanoparticles (-15 to -25 kcal/mol peptide). Binding and selectivity appear to be controlled by the size of surface features and the extent of co-ordination of epitaxial sites by polarizable atoms (N, O, C) along the peptide chain. The adsorption energy of a single peptide equals a fraction of the sum of the adsorption energies of individual amino acids that is characteristic of surface shape, epitaxial pattern, and conformation constraints (often β -strand and random coil). The proposed adsorption mechanism is supported and critically evaluated by earlier sequence data from phage display, dissociation constants of small proteins as a function of nanoparticle size, and observed shapes of peptide-stabilized nanoparticles. Understanding the interaction of single peptides with shaped metal surfaces is a key step towards control over self-organization of multiple peptides on shaped metal surfaces and the assembly of superstructures from nanostructures.

Dr. J. Feng, Prof. H. Heinz
Department of Polymer Engineering
University of Akron
Akron, OH 44325-0301, USA
E-mail: hendrik.heinz@uakron.edu

Dr. J. M. Slocik, Dr. R. R. Naik, Dr. B. L. Farmer
Materials and Manufacturing Directorate
Air Force Research Laboratory
Wright Patterson Air Force Base, Dayton, OH 45435, USA

Prof. M. Sarikaya
Department of Materials Science and Engineering, GEMSEC
University of Washington
Seattle, WA 98195, USA

DOI: 10.1002/smll.201102066



1. Introduction

Self-assembled nanostructures of metals, biomolecules, and surfactants have shown promise for a wide range of applications, including miniature electronic and optical devices, sensors, catalysts, tissue markers, and carriers for drug delivery.^[1–11] The combination of peptides with specific recognition properties and metal nanostructures with specific conductive and reactive properties enables new circuitry, sensor functions, chemical reactivity, and therapeutics.^[5,6,9–14] For example, gold nanorods can assemble into loops and wires by decoration with suitable surfactants,^[5] specific detection of molecules becomes possible by changes in the plasmon resonance frequency of gold nanorods modified with proteins.

Photothermal cancer therapy relies on specifically decorated gold nanostructures which selectively bind to tumor cells and destroy the tumor cells by laser-induced local heating.^[8]

Peptide templates have been extensively employed to control the growth rate, size, and shape of metal nanostructures.^[10–17] It remains difficult, however, to monitor and understand the hidden metal-biological interfaces at the nanometer scale.^[1–30] The influence of particle size and surface shape on adsorption of single and multiple peptides are still unclear, and observations of particle growth, shape control, and catalytic function still leave many open questions. To monitor interfaces at the nanometer scale and identify some of the underlying mechanisms, molecular simulation along with interpretation and validation in the context of measurements can be a valuable tool.^[10,12,31–51]

Adsorption of organic molecules on even metal surfaces in solution has been shown consistently by simulation and experiment to involve largely non-covalent coordination of polarizable atoms (N, O, C) to multiple epitaxial sites,^[44,51] which is complemented by the attraction of strongly ionic groups by induced charges^[50] and covalent bonding of thiols. The approximate number and strength of simultaneous epitaxial contacts under the influence of conformational constraints determines the adsorption energy of solute versus solvent molecules. This geometry-controlled adsorption mechanism is related to the high surface energy of metals in comparison to lower surface energies of oxide and polymer surfaces. The sub-Angstrom location of polarizable atoms with respect to epitaxial sites still remains difficult to trace directly by imaging techniques^[9–11,14,15,18] or by high-level quantum-mechanical calculations (MP2 or CASSCF).^[46]

Simulation approaches range from quantum-mechanical approaches and classical atomistic energy models to coarse-grain models and combinations of methods. Quantum-mechanics permits the analysis of adsorption of single molecules on metal surfaces in vacuum,^[31–33,36–41] including coordination geometry, charge transfer, and reactivity.^[36–38, 41,50,52,53] However, properties in the gas phase differ greatly from those in solution, and the simulation of a significant number of gold atoms, water molecules, and amino acids in the liquid state by ab-initio methods is limited by $O(N^3)$ to $O(N^7)$ scaling with the number of electrons N and by major sacrifices in the accuracy of the wave function.^[36,46] Compared to ab-initio methods, molecular dynamics simulation (MD) with a classical force field is better suited because the Hamiltonian allows an increase in system size from 10^2 to 10^5 atoms and in time scale from 10^{-12} s to 10^{-6} s. These extended time and length scales allow the analysis of adsorption equilibria involving solutes and thousands of solvent molecules, examinations of the influence of ionic concentration and of pH.^[44,45] The simplified energy expression does not model the formation of covalent bonds yet, favorably, the presence of a dense, multipolar solution of solvent molecules and biopolymers on the metal surface leads to a strong reduction of covalent bonding contributions compared to the gas phase due to high coordination numbers of all gold atoms, including exposed atoms at edges and in small metal clusters (<100 atoms).^[18,31,41,44,46,51] Coarse-grain models^[42,47] are

also available, even though further simplification of chemical details therein limits molecule-specific insight.

The quality of results from atomistic simulations depends on the force field. We previously developed and validated the CHARMM^[54]-METAL^[55] force field which combines optimized Lennard-Jones parameters for elemental metals^[55] with excellent parameters for biomolecules^[54] (see documentation in refs. 51, 54, 55, and methods section). The metal parameters reproduce densities in 0.1%, surface energies of different crystal faces in 2%, and interfacial properties such as water layering, dielectric constants in water layers, and interface tensions in 10% agreement with experiment.^[50,51,55] Previous MD simulations using the CVFF-METAL^[42,44,50] and CHARMM-METAL^[51] force fields explained the relative adsorption of single amino acids and peptides on even gold and palladium surfaces in agreement with numerous laboratory observations.^[5–30] For example, high affinities of peptides to Au {111} surfaces, lesser affinity to Au {100} surfaces, the relative adsorption strength of 20 amino acids in comparison to sequence information from phage libraries, and available ab-initio data^[36,38,46] have been consistently explained.^[44,51] As the metal parameters in the CHARMM-METAL force field perform well for different Miller planes with deviations in the small percent range,^[55] we investigated the influence of differently shaped gold surfaces on peptide adsorption using this model. As an alternative, reactive force fields could also be employed.^[48,56] However, the current quality of metal parameters in reactive force fields is lower than in CHARMM-METAL^[56,57] and compatibility with high quality parameters for biomolecules (CHARMM, AMBER, OPLS-AA) is missing. In addition, the computational expense would be $\sim 10^3$ times higher compared to classical force fields.

To probe the influence of surface shape on adsorption, we employed models of four peptides (**Table 1**) in aqueous solution in contact with (i) an even Au {111} surface of $3.5 \times 4.0 \text{ nm}^2$ area, (ii) an even {111} surface containing two vertical steps of 0.7 nm height and 1.7 nm lateral separation that are bounded by {1–10} surfaces, and (iii) a Wulff-shaped cuboctahedral nanoparticle of 2.0 nm diameter bounded by {111} and {100} facets (**Figure 1**). The surfaces were brought into contact with single peptide molecules in the presence of 2000 explicit water molecules at pH = 7 under 3D periodic boundary conditions (28 mM). As single peptide molecules in the simulation box hardly interacted with periodic images, the corresponding effective concentration was between 28 mM and infinite dilution (see methods section for details).

The peptides were selected to represent strong attraction, intermediate attraction, and template functions in nanoparticle synthesis (Table 1). The homopeptide Tyr₁₂ was

Table 1. Peptide names, sequences, and charge state at pH = 7 in the simulation.

Name	Peptide Sequence
Tyr ₁₂	(+)YYYYYYYYYY(–)
Ser ₁₂	(+)SSSSSSSSSS(–)
A3	(+)AYSGAPPMPF(–)
Flg-Na ₃	(+)(–)DYK(+)(D(–)D(–)D(–)K(+)(–) • 3 Na (+)

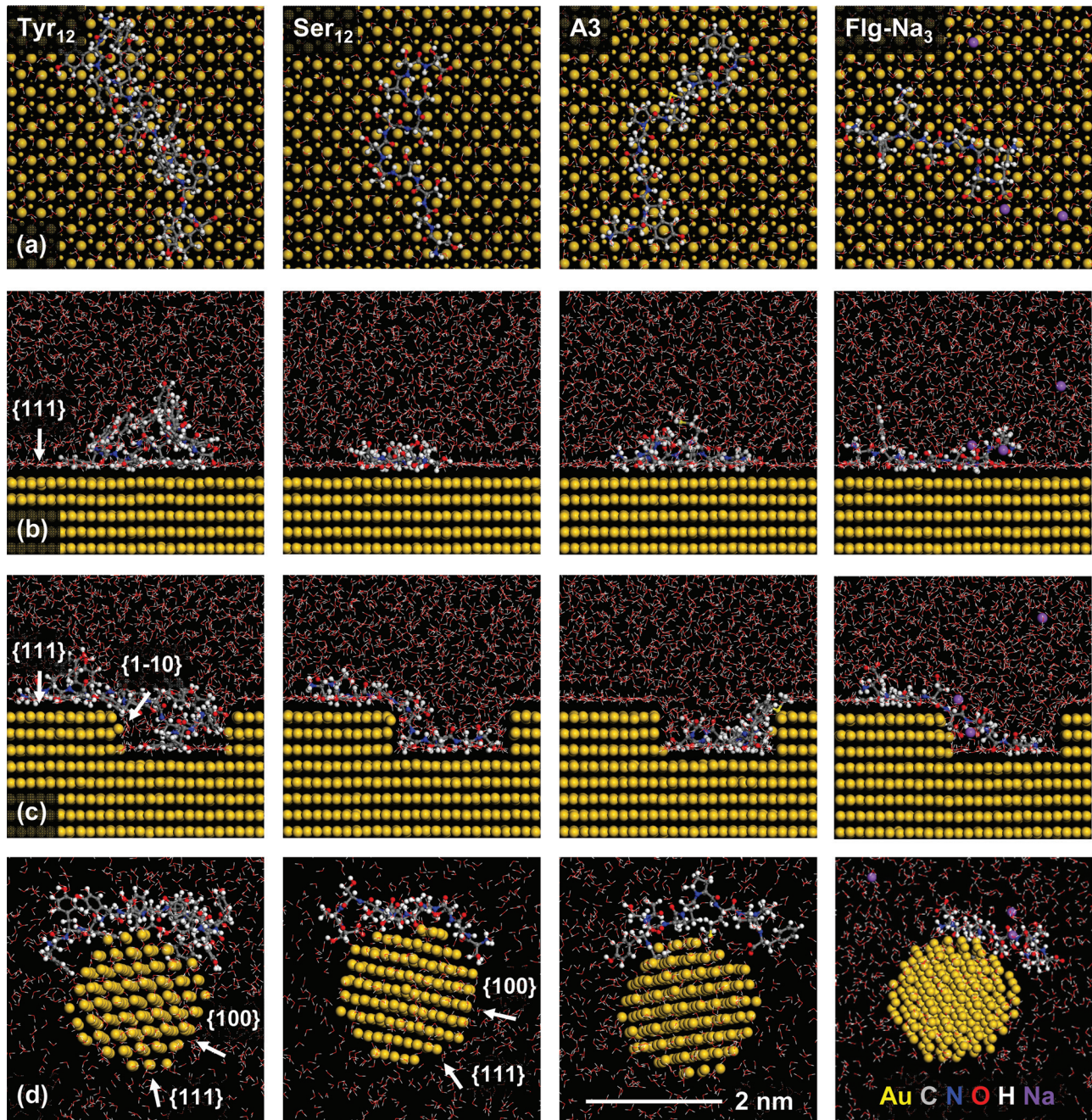


Figure 1. Representative snapshots of the peptides Tyr_{12} , Ser_{12} , A3, and Flg-Na_3 adsorbed on differently shaped gold surfaces. (a,b) Even Au {111} surfaces in top and side view, (c) stepped surfaces, and (d) a cuboctahedral nanoparticle of 2 nm diameter bounded by {111} and {100} surfaces. On even surfaces (a), polarizable atoms in sp^2 and sp^3 hybridized groups in the peptide backbone (N, O, C) coordinate with subjacent atomic layers (indicated as smaller spheres and crosses) and avoid Au atoms of the top layer (indicated as larger spheres). (b) Large portions of the peptide molecules are in direct contact with the metal surface ($<3\text{\AA}$ distance from the top layer of Au atoms) causing strong, sequence-selective adsorption. Stepped surfaces (c) show similar features, including geometrically enhanced adsorption near the inner edge and less favorable adsorption near the outer edge. On small cuboctahedral gold nanoparticles (d), the size of the facets is reduced and the geometric fit of polarizable atoms to epitaxial sites on {100} facets is weaker compared to {111} facets. More water molecules enter between the nanoparticle surface and the peptide, resulting in weaker adsorption on time average.

chosen in expectation of strong adsorption to even Au {111} surfaces. The amino acid Tyr is frequent in strongly binding peptide sequences identified by phage display,^[14,16,28] enables the synthesis of Au nanoparticles from HAuCl_4 ,^[15] and binds strongly to gold surfaces in simulations.^[51] The homopeptide Ser_{12} was chosen in expectation of intermediate adsorption.

We often found Ser in gold-binding peptides while it does not appear to be a main driver for adsorption.^[17,21] Phage libraries^[28] and simulations^[51] indicate some attraction to gold surfaces. The neutral peptide A3 was chosen due to strong adsorption on all of Ag {111}, Au {111}, and Pd {111} surfaces in phage display,^[16,17,21] consistent with similar lattice

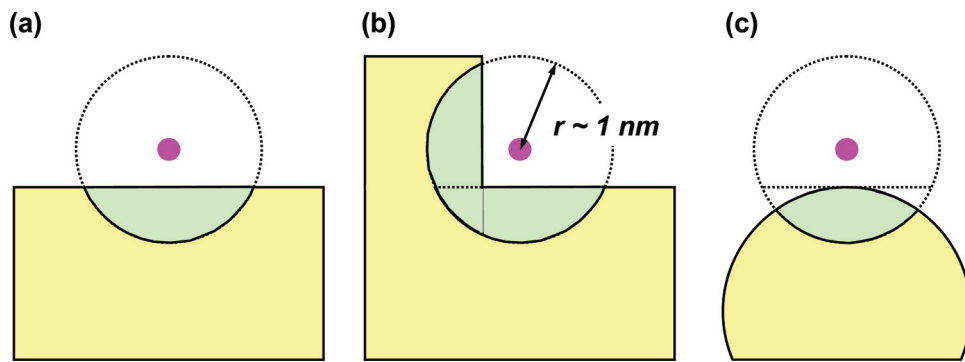


Figure 2. Simplified illustration of the size of surface features (yellow) and their contribution to noncovalent adsorption (green) of a probe atom (pink) in solution, shown in 2D. Chain molecules can be envisioned as a collection of connected probe atoms. The probe atom exhibits a certain adsorption (green) on the even surface (a), stronger adsorption on the inner edge of a stepped surface (b), and weaker adsorption on a curved surface (c). Adsorption is further affected by different bounding facets {x y z} and competition between solute and solvent molecules. Covalent bonding tendencies of the probe atom at outer edges and at surfaces of small nanoparticles in vacuum are reduced by immersion of the metal nanostructures in solvent.^[41]

spacing of these metals and soft epitaxial adsorption.^[18,44,51] Besides, peptide A3 formed stable Au nanoparticles from HAuCl₄ precursor solutions^[17] as well as Au-Pd bimetallic structures.^[21] The threefold negatively charged peptide Flg-Na₃ is a common antibacterial polypeptide tag^[57] which also supports the formation of gold and Au-Pd bimetallic nanoparticles from ionic precursors (Table 1).^[17,21]

2. Results and Discussion

2.1. Surface Shape and Peptide Attraction

The nanostructured metal surfaces differ in the size of surface features and in the arrangement of epitaxial sites (Figure 1 and **Figure 2**). Extended metal surfaces of multilayer thickness (>2 nm) enable the full range of interactions with adsorbed probe atoms or chain molecules. This long range of interactions enables strong attraction when molecule conformations facilitate a good epitaxial match (Figure 2a). Inner edges of stepped surfaces may be even more attractive due to the presence of more metal atoms within the range of intermolecular interactions of the probe atom or of a chain molecule (Figure 2b). Surfaces with a radius of curvature smaller than the persistence length of the chain molecule, or smaller than the range of intermolecular interactions, will be less attractive than even surfaces (Figure 2c).

This simple view coincides with experimental observations of adsorption strength and sequence selectivity. Supporting data and uncertainties are discussed in Section 3, *Comparison to Experiments* as well as in the Supporting Information.^[5,6,9,10,11,13–19,21,28–30] A more refined model for specific surface attraction can be obtained taking into account specific Miller planes {x y z} and epitaxial sites. We employed the surface potential, i.e., a two-dimensional map of the adsorption energy of a probe atom relative to vacuum, which is shown for the same shaped gold surfaces (**Figure 3**). A single carbon atom served as a probe atom and was moved in high resolution across the metal surface bounds at a constant distance of 3 Å from the top atomic layer.^[58] The

attraction of chain molecules, instead of a probe atom, can be envisioned by the corresponding framework of atoms and its ability to coordinate multiple epitaxial sites. The greater the ability to adjust the conformation such that many polarizable atoms are close to sites of low surface potential, the stronger would be the adsorption of the chain molecule.

On the even Au {111} surface, the surface potential shows a hexagonal spacing of attractive sites (green) of 1.66 Å with -4 kcal/mol attraction and also a hexagonal spacing of energetically less favorable sites at top layer atoms (yellow) of 2.88 Å with -2.7 kcal/mol attraction (Figure 3a). On the surface containing a three-atom step of 7 Å depth, the inner edge is most attractive (blue) with -6 kcal/mol and the outer edge is least attractive (red) with only -0.5 kcal/mol (Figure 3b). The faceted nanoparticle of 2 nm diameter in comparison to even and stepped surfaces displays a throughout higher (closer to zero) surface potential above -2.1 kcal/mol (Figure 3c). The epitaxial pattern is also weaker, related to smaller size and higher curvature.

2.2. Computed Adsorption Energies and Binding Mechanism

The trends in surface potential are reflected in the adsorption energies of the peptides by molecular dynamics simulation (**Figure 4**). For the same peptide, strongest adsorption is found on stepped and even surfaces, and less adsorption on the spherical nanoparticle (Figure 1). On the same surface, the relative affinity among different peptides is determined by competition between peptide residues and water molecules for epitaxial sites as well as possible differential stabilization of the peptides away from the surface in solution.

On even and stepped {111} surfaces, polarizable atoms (N, O, C) in planar sp² hybridized side groups as in Tyr₁₂, or in sp³ hybridized groups as in Ser₁₂, achieve a good fit to multiple epitaxial sites and lead to low (far below zero) adsorption energy (Figure 1a, 1b). On the stepped surfaces, the inner edge of lowest surface potential remains mostly in contact with small water molecules and not with peptide, as simulations with many peptide orientations relative to the

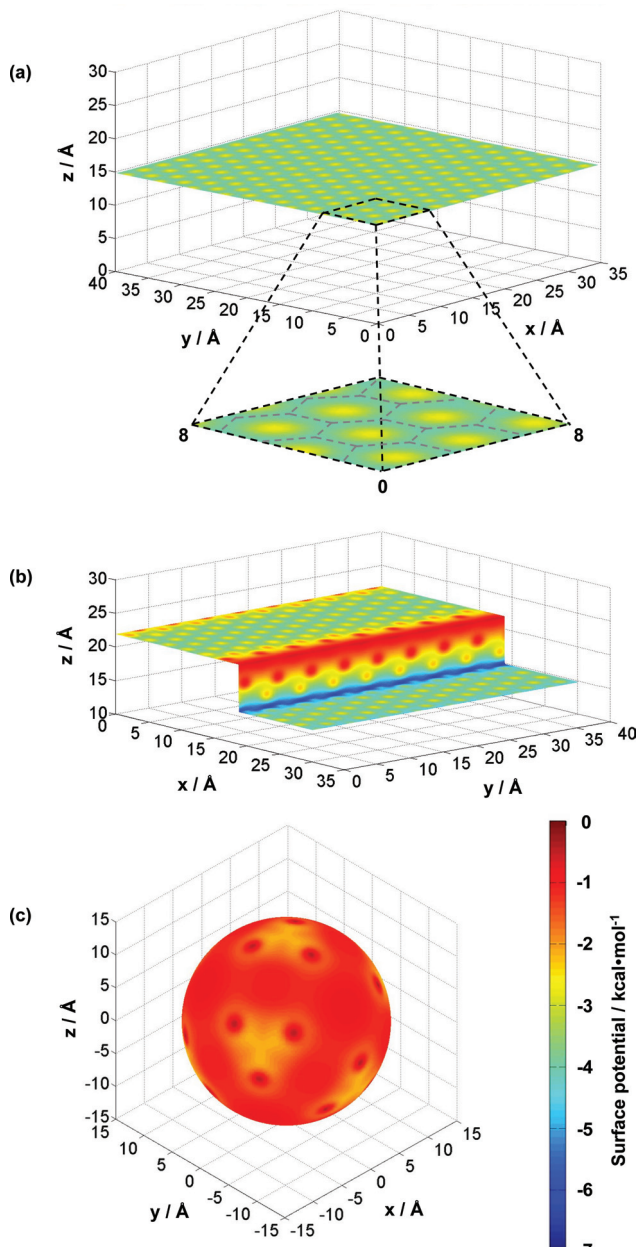


Figure 3. Surface potential of nanostructured gold surfaces. The color code indicates the attraction of a carbon probe atom at a fixed distance of 3 Å apart from the top layer of metal atoms.^[58] Blue and green regions are more attractive than yellow, red, and brown regions and preferably coordinate polarizable atoms (N, O, C) in solute and solvent molecules. (a) Even {111} surface with a hexagonal pattern of epitaxial sites, highlighted in the zoomed region by gray dashed lines, (b) a step of 7 Å bounded by {111} and {1-10} surfaces with locally modified hexagonal patterns, (c) a cuboctahedral nanoparticle of 2.0 nm diameter bounded by eight orange colored {111} facets and six darker colored {100} facets. The nanoparticle displays weaker and less well structured adsorption sites.

step indicate (Figure 1c). This is associated with the excluded volume at the metal edge and the spatial demand of the peptide. Even when peptides were initially oriented along the inner edge in the simulation, the majority of residues moves toward adjacent confining walls and few peptide residues remain in close contact with the edge.

On the faceted surface of the 2 nm sized nanoparticle, polarizable atoms in the peptides cannot achieve an optimum fit due to the small particle size near the range of intermolecular interactions (Figure 2c), as well as the curvature with alternating {111} and {100} facets (Figure 1d). In particular, the {100} facets on the cuboctahedral surface hardly attract the peptides.^[44] On time average, partial detachment of amino acid residues occurs, more mobile water molecules coordinate with the nanoparticle surface (including atoms in the top layer^[46]), and adsorption energies of the peptides increase (less below zero) compared to even and stepped surfaces.

On all surfaces, adsorption energies of the peptides are higher (less below zero) than the sum of adsorption energies of constituting amino acids on even {111} Au surfaces (Figure 4). This is related to conformational constraints, and particularly Tyr₁₂ with large side groups adsorbs only 30% as strongly in comparison to twelve individual Tyr residues in high dilution.^[51] The fraction of peptide adsorption energy in relation to the sum of adsorption energies of individual amino acids can, in principle, also exceed one^[44] and is a function of the surface shape, epitaxial pattern, and conformational flexibility of the peptide.

The affinity of different peptide sequences to even surfaces decreases in the order Tyr₁₂ > Ser₁₂ > A3 > Flg-Na₃, whereby Flg-Na₃ is significantly less attracted than the other peptides. The affinity of all peptides to the stepped surface is high although the sequence selectivity appears lower in comparison to the even surface. The affinity decreases slightly in the order Tyr₁₂ > Ser₁₂ > (A3, Flg-Na₃) within the error bars, whereby Flg-Na₃ is clearly more attracted to the stepped surface than to the even surface. The affinity to the cuboctahedral nanoparticle is (Tyr₁₂, A3, Ser₁₂) > Flg-Na₃. The curved surface, therefore, exhibits the lowest sequence selectivity among all surface types, as well as diminished (less below zero) adsorption.^[6,9]

The energy of adsorption is in good approximation equal to the free energy of adsorption since the loss in conformational flexibility of the peptides upon adsorption is largely offset by release of surface-bound water molecules.^[44,51] Using histogram methods for selected cases, we identified small positive entropy contributions, $-T\Delta S$, which increased \bar{A}_{Ads} (less below zero) relative to \bar{E}_{Ads} (further below zero) uniformly by about 5%.

2.3. Conformations on Even, Stepped, and Curved Surfaces

On the even gold {111} surface, the backbone of Tyr₁₂ resembles a β -strand with local disorder (Figure 1a and 1b). Partial coiling occurs as a result of conformational constraints by the large side groups and intra-chain interactions between aromatic rings. 4 to 5 Tyr residues are in direct contact with the surface on time average and the aromatic side groups coordinate multiple epitaxial sites. The binding energy equals 30% of the sum of the binding energies of 12 individual Tyr monomers.^[51] The conformation of the Ser₁₂ backbone is flexible in aqueous solution and folds on the even Au {111} surface to coordinate subjacent atomic layers (Figure 1a). Thereby, CH₂OH side groups avoid proximity to the top Au

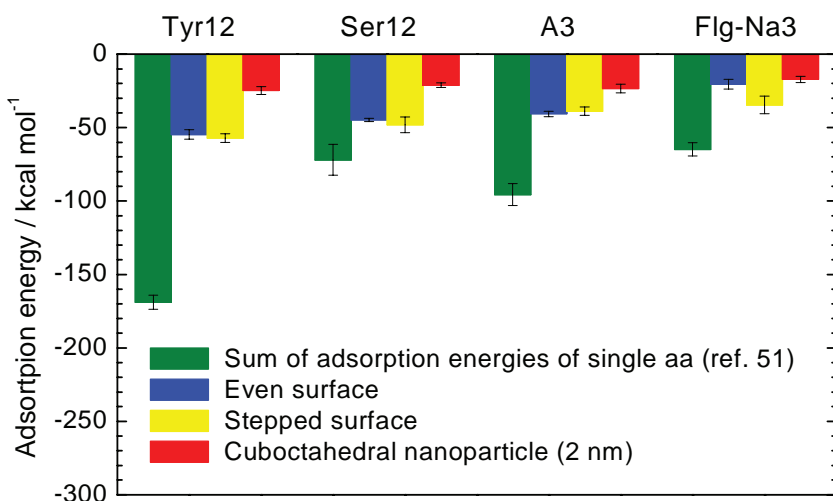


Figure 4. Computed adsorption energy of single peptides in aqueous solution on even {111} surfaces, {111} surfaces with 3-atom steps, and a cuboctahedral nanoparticle of gold using molecular dynamics simulation with the CHARMM-METAL force field. Even surfaces show strong and selective adsorption in the order $\text{Tyr}_{12} > \text{Ser}_{12} > \text{A3} > \text{Flg-Na}_3$. Selectivity is weaker on stepped surfaces. Weakest and least selective adsorption was found on the 2 nm sized cuboctahedral nanoparticle.

atomic layer (Figure 1a, b). 7 to 10 Ser residues are in direct contact with the even surface on time average. The binding energy equals 65% of the sum of the binding energy of 12 individual Ser residues (Figure 4) and conformations are randomly distributed in the $\Phi - \Psi$ space. The heteropeptides A3 and Flg-Na₃ exhibit substantial surface contact with 5 to 8 residues and the adsorption energy is less than 50% of the sum of adsorption energies of the individual amino acids (Figure 4).^[51] A3 and Flg-Na₃ prefer conformations close to β -strands on the even surface.^[44]

On the stepped surface, more residues of Tyr₁₂ are in direct contact compared to the even surface, supported by conformational constraints. The backbone was shaped predominantly as a β strand. In Ser₁₂, 8 to 11 residues are close to the surfaces of the confining walls of the inner edge and conformations are scattered in $\Phi - \Psi$ space. Peptide A3 displayed no major adaptive changes compared to the even surface, and peptide Flg-Na₃ shows more proximity to the stepped surface compared to the even surface (Figure 1c). A3 and Flg-Na₃ retain predominantly β strand conformations. For all peptides, attraction to the outer edge (step edge) is lower than to the inner edge due to a lower number of coordinating metal atoms and higher surface potential (Figures 2b and 3b).

On the faceted nanoparticle, a loss of direct contact of the metal surface with peptide residues was observed in favor of more solvent adsorption (Figure 1d). Tyr₁₂ shows 2 to 6 residues close to the surface of which approximately two are oriented parallel and others perpendicular to the surface, commensurate with their preferences on {111} and {100} facets, respectively. Ramachandran analysis indicated a distorted β strand. Ser₁₂ exhibits 7 to 10 residues in close contact with the surface and backbone dihedral angles are distributed in the $\Phi - \Psi$ space with a tendency toward an α -helix in less attached conformations. A3 and Flg-Na₃ peptides show proximity of 2 to 5 residues to the surface, and Met of A3 was

seen close to the surface. Tyr and Phe residues preferred non-parallel orientations to the surface. Conformations of A3 and Flg-Na₃ were close to β strand.

3. Comparison to Experiment

Direct experimental insight into the adsorption of single peptides on metal surfaces remains difficult to obtain.^[18] Yet, numerous data from phage display provide information on sequence-specific attraction of peptides to even and stepped metal surfaces,^[10,11,16,17,21,28-30] binding constants of small proteins to nanoparticles of various size and shape have been quantified,^[6,9,17] and observations of sequence-specific stabilization of nanoparticles in solution have been made.^[10,11,15,17] While there are many factors involved in adsorption and nanoparticle stabilization, the comparison of these observations to the simulation of single peptides on

shaped metal surfaces indicates qualitative and quantitative trends. The interpretation supports that particle stabilization and binding constants depend on the size of surface features and epitaxial patterns. In the following, we will discuss individual evidence and limitations.

3.1. Sequence-Specific Peptide Adsorption on Extended Facets

Independent combinatorial studies report the high affinity of Arg, Tyr, and Trp residues to {111} surfaces.^[14,16,28] Other studies also mention His, Gln, Met, and Phe^[13,19,29,30] as residues with significant binding to gold {111} surfaces. Although sometimes multiple peptides may be attracted to the surface in phage display, the observed order of attraction of amino acids is in very good agreement with the computed order using the CHARMM-METAL force field.^[51] Also, the experimentally observed attraction of peptides to {111} surfaces and the absence of attraction of the same peptides to {100} surfaces was seen by simulation and attributed to soft epitaxy.^[44] The observation that peptide A3 binds to Ag {111}, Au {111}, and Pt {111} surfaces about equally strongly^[16,17,21] can be effortlessly explained with a soft epitaxial adsorption mechanism since the lattice spacing L1 on Ag, Au, and Pd {111} surfaces is very similar (1.668, 1.665, and 1.588 Å).^[51] This mechanism has been extensively described with more supporting observations in refs. 44, 50, and 51. To the best of our knowledge, no disagreement or limitations were reported to date.

3.2. Peptide Adsorption on Nanoparticles of Various Size

Two independent studies report a decrease in protein dissociation constants by two to three orders of magnitude when the size of gold nanoparticles increased from small sizes of 2

to 5 nm to >50 nm.^[6,9] Six different small proteins in the two binding studies also showed a gain in sequence selectivity towards the larger nanoparticles.^[6,9] Both observations are fully consistent with the gain in adsorption and in sequence recognition of the four peptides in the simulation from the 2 nm cuboctahedral nanoparticle towards extended {111} surfaces (see detailed comparison in section S1 of the Supporting Information). Whereas small cuboctahedral particles are of the same size as the proteins and bounded by a combination of {111} surfaces and less attractive {100} surfaces, large particles are predominantly bounded by thermodynamically stable {111} facets which exceed the size of the protein and can be regarded as even {111} surfaces in first order. As a result, the adsorption energy decreases (further below zero) and the protein selectivity increases from smaller nanoparticles towards larger nanoparticles.

3.3. Shape of Gold Nanostructures

Several studies report on the influence of peptides on the size and shape of metal nanostructures synthesized from metal salts in solution.^[10,11,17,59] A minimum size of nanoparticles appears to be required for stabilization by peptides to become effective and lock nanoparticle growth,^[10] and also the selective recognition of facets plays a major role to develop a specific shape.^[11] Both observations are consistent with our suggested model. Specifically, the peptides A3 and Flg-Na₃ have shown distinct effects in the synthesis of gold nanoparticles that correlate with computed adsorption energies (Figure 4).^[17] Peptide A3 leads to approximately spherical Au nanoparticles (diameter 12.8 ± 2.9 nm) and peptide Flg-Na₃ leads to irregularly shaped nanoparticles containing steps (size 13.3 ± 7.4 nm) upon synthesis from HAuCl₄ in aqueous solution using the peptides as a mild reducing agent.^[17] In the simulation, A3 was about equally attracted to even and stepped surfaces so that the formation of sizeable (13 nm) particles bounded mostly by {111} facets appears favorable. Flg-Na₃ was more attracted to stepped surfaces so that the stabilization of irregular stepped surfaces also appears supported. Undoubtedly, there are many competing interactions in nanoparticle synthesis, although ultimately particles appear to be stabilized and locked from further growth by the peptides or other stabilizers.^[10,11] The prospect to explain and potentially predict nanoparticle shape and assembly using simulation tools is exciting (see a further example of nanorod assembly in section S2 of the Supporting Information^[5]). Meaningful interpretations and the anticipation of trends have also been demonstrated in previous studies.^[44,50,51]

4. Conclusion

We examined the relation between the shape of a metal surface and the adsorption mechanism of peptides in aqueous solution using molecular dynamics simulation with the CHARMM-METAL force field. The size of surface features in combination with the pattern of epitaxial sites characterizes the attraction of biomolecules in competition with

solvent molecules. The surface potential represents these details of a given surface and can provide guidance in the design of complimentary molecules. Thereby, coordination of multiple polarizable atoms (N, O, C) in a given peptide molecule to epitaxial sites increases adsorption. {111} facets on even and stepped surfaces lead to stronger and more selective adsorption of peptides whereas small, cuboctahedral nanoparticles containing {111} and {100} facets on the surface lead to weaker and less selective adsorption. Adsorbed peptides typically exhibit β strand or random backbone conformations. Adsorption energies are a fraction of the sum of adsorption energies of corresponding single amino acids which reflects conformational constraints and surface characteristics. Consistency of the proposed adsorption mechanism with earlier measurements of peptide adsorption on nanoparticles of different size and shape has been shown. Accordingly, soft epitaxy appears to dominate self-assembly at metal interfaces in solution unless covalently bonding groups (thiols, selenols) or strongly ionic groups are present.^[50] The computational method demonstrated the potential to answer open questions in anisotropic growth, shape control, and assembly of metal nanostructures, as well as to rationally select molecules that match to specifically shaped metal surfaces.

5. Models and Methods

Models: The models consist of gold surfaces, single peptide molecules in zwitterionic form at pH = 7 (Table 1), and 2000 pre-equilibrated water molecules in all atomic resolution under 3D periodic boundary conditions. The even Au {111} surface had a cross-sectional area of 34.608 Å × 39.960 Å and a thickness of 14.128 Å. $\sqrt{3} \times 22$ surface reconstruction was neglected due to the limited dimension of the simulation box and for facile model reproducibility.^[60–62] The stepped surface was prepared from the even {111} surface by an increase in thickness to 21.192 Å and abscission of a vertical step of 7.064 Å height and 17.304 Å length along the x direction (width 39.960 Å). The vertical wall in this designed morphology is a {1–10} surface which has no specific defects but reconstructs to some extent in the simulation (Figure 1c). The cuboctahedral nanoparticle was prepared from bulk Au by selection of a center atom and application of a spherical cutoff to all atoms at >1.0 nm distance. The nanoparticle was bounded by {111} and {100} facets, contained 249 atoms, and had a diameter of 2.01 nm on the basis of total atomic volume. The shape was maintained after annealing in vacuum (e.g., at 600 K) and upon equilibration in aqueous solution in a simulation box of 34.506 × 34.506 Å² dimension in the xy plane. The cuboctahedral shape corresponds to the Wulff equilibrium and was also observed by TEM of small nanoparticles.^[10,11]

For the computation of the surface potential, an aromatic carbon atom was placed on top of each of the three different metal surfaces and moved across the surface bounds at a fixed distance of 3.0 Å from the top atomic layer (Figure 3).^[58] The same atom was also placed at a distance of 30 Å away from each surface to define a reference energy of zero.

For the computation of the adsorption energy of the peptides, five to seven independent simulations were carried out for each

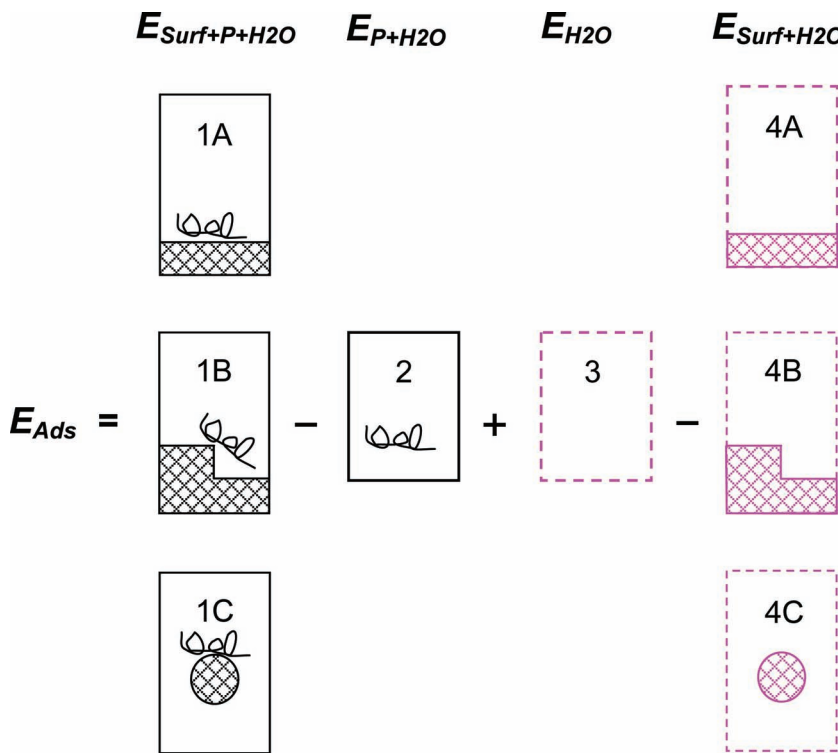


Figure 5. Computation of the adsorption energy of peptides on differently shaped metal surfaces in aqueous solution. For each peptide-surface combination, four simulations were carried out including a surface-peptide-water, peptide-water, water, and surface-water system. The systems highlighted in pink contain no peptide and, therefore, accelerate the screening of multiple peptides and different peptide conformations on the same surface.^[45]

combination of surface and peptide using the CHARMM-METAL force field, and another five to seven simulations using the CVFF-METAL force field. Each combination included a metal-peptide-water system ($E_{Surf+P+H_2O}$), a peptide-water system (E_{P+H_2O}), a metal-water system (E_{Surf+H_2O}), and a water only system (E_{H_2O}) for reference (Figure 5).^[45] The dimension of all simulation boxes in z direction was adjusted to a constant density of 1000 kg/m³ in the aqueous phase. The total volume consisted of the volume of the aqueous phase, the volume of the peptide (at 1000 kg/m³), and the volume of Au atoms. For the metal-peptide-water systems and the peptide-water systems, ten to fourteen independent simulations started with different initial peptide conformation (β strand, α helix, random coil, different orientation relative to the surface) to achieve convergence in conformation sampling. All model structures were prepared using the graphical interfaces of Hyperchem^[63] and Materials Studio.^[64]

Energy Expression: As briefly described in the introduction, modeling self-assembly processes in aqueous solution necessitates the inclusion of chemically specific interactions in the model such as long range ionic interactions, hydrogen bonds, pH, and realistic peptide concentrations. Also, length scales of multiple nanometers and time scales far beyond nanoseconds are essential to analyze interfacial structures and adsorption mechanisms.^[44,45,51] A suitable and feasible approach is classical molecular dynamics simulation in all-atomic resolution, which strikes a balance between computationally demanding electronic structure calculations and chemically nonspecific coarse-grain simulations.^[42]

The CHARMM-METAL force field^[51] was previously developed under consideration of thermodynamic consistency between the organic and inorganic components^[65–67] which enables the quantitative analysis of interfacial structure and dynamics.^[44,50,51,68–70] Fcc metals are described by Lennard-Jones (LJ) parameters.^[55] Although approximate and sacrificing the electronic structure, the LJ parameters were designed to reproduce densities and surface energies of various fcc metals in quantitative agreement with experiment (<2% deviation) under ambient conditions.^[55] As a simple geometric consequence, surface energies of different crystal faces such as {111}, {100}, and {110} are also reproduced in proportion to each other within the experimental uncertainty, and the parameters are consistent with the energy expression of biomolecular force fields including CHARMM, AMBER, and OPLS-AA.^[55] The performance of the LJ parameters in metal surface properties exceeds that of customized embedded atom models^[48,56] and equals current ab-initio methods.^[48] Elastic moduli of the metals are also computed within ~20% of experimental values. Interesting questions for further work are posed by the impact of reconstruction on {100} and {111} surfaces which we have not yet taken into consideration. The periodic repeat patterns often extend over many

nanometers and depend on the process history.^[60]

The CHARMM-METAL force field reproduces the layered structure of metal-water interfaces and adsorption energies of the 20 single amino acids in solution in good agreement with experiment.^[50,51] Computed interface tensions with water^[55] and the stepwise decrease of the dielectric constant near the surface deviate <10% from experiment.^[50,55] The quality of the CHARMM-METAL force field and the difficulty to carry out high-level electronic structure simulations make it suitable to simulate interfaces of biomolecules with metal nanostructures of different geometry and crystallographic facets in solution.

As mentioned, a main limitation is the neglect of the formation of covalent bonds. Covalent bonding may play a major role between small molecules and metal surfaces in vacuum, especially at edges and in small metal clusters due to Smoluchowski smoothing.^[31,41] Therefore, the force field is of limited use for such systems without specific modifications. In contrast, covalent bonding is a minor contribution in aqueous solution and in other condensed phases where the assembly of biomolecules and nanoparticles commonly occurs. The coordination number of all metal atoms is then similarly high and the decreased importance of covalent bonding is supported by vacuum studies with increasing surface coverage^[18,41] and electronic structure calculations on small subsystems of peptides (excluding Cys), water molecules, and metal surfaces.^[35,37,45] We also found good agreement between computed adsorption energies using force field (CVFF^[71]-METAL^[55]) and ab-initio methods.^[44] We also employed the two independent force fields CHARMM^[54]-METAL^[55] and CVFF^[71]-METAL^[55] for all

calculations (see Supporting Information). These force fields combine the accuracy and functionality of biomolecular force fields^[54,71] with that of accurate parameters of elemental metals^[55] whereby the CHARMM-METAL force field is preferred over the older CVFF-METAL force field.

Simulation Protocol: The computation of the surface potential (Figure 3) involved approximately one million single point energy calculations of the probe atom on the surface bounds of each metal nanostructure at a distance of 3 Å, as well as a reference calculation at 30 Å distance from the surface of each metal nanostructure to define a zero energy level. The position of the probe atom was changed in steps of 0.1 Å to obtain a two-dimensional or three-dimensional map of the surface potential, respectively.

Simulation of the interfacial structures and adsorption energies of peptides (Figures 1, 4, and S1) involved molecular dynamics simulation (MD) in the NVT ensemble at a temperature of 298.15 K, using the Verlet integrator, a time step of 1 fs, summation of van-der-Waals interactions using a spherical cutoff at 1.2 nm, and a summation of Coulomb interactions using the particle-particle-particle-mesh (PPPM) method with a high accuracy of 10⁻⁶ kcal/mol. The summation of Coulomb interactions in high accuracy is slow but essential to compute reliable adsorption energies. All atoms were free to relax. Each system was equilibrated for 0.4 ns and then subjected to 1 ns simulation time to collect 2000 snapshots and thermodynamic data for analysis. The cumulative simulation time was 14 to 20 ns for each surface-peptide combination in ten to fourteen independent simulations. Simulations using CHARMM-METAL were carried out using the program NAMD^[72] and simulations using CVFF-METAL using the program LAMMPS.^[73]

Analysis: The analysis involved the visual inspection of peptide conformations at the metal surfaces and in solution. We computed Ramachandran plots (not shown) and adsorption energies. The adsorption energy for each surface-peptide-water combination was obtained using a compartmentalization method with modifications for shaped surfaces (Figure 5):^[45]

$$E_{Ads} = E_{Surf + P+H_2O} - E_{P+H_2O} + E_{H_2O} - E_{Surf + H_2O} \quad (1)$$

Thereby, the uncertainty in the reference simulations $E_{Surf + H_2O}$ and E_{H_2O} was less than 1 kcal/mol and the uncertainty in E_{P+H_2O} only ~1 kcal/mol, corresponding to a high level of conformation and energy convergence by use of different start structures of the peptide in solution. The energies of the surface-peptide-water system $E_{Surf + P+H_2O}$, however, varied between simulations with independent initial conformations between 2 and 5 kcal/mol and were the major source of uncertainty. Yet, conformation convergence of the peptides on the surface and the uncertainty in $E_{Surf + P+H_2O}$ were good in comparison to total adsorption energies between -20 and -50 kcal/mol. Longer simulation times (up to ten times) had nearly no effect due to very strong adsorption. Convergence was optimized using many independent start configurations and comparatively short simulation times, as well as brief annealing at higher temperature to overcome energy barriers. In the determination of the average adsorption energy \bar{E}_{Ads} , the simulation of highest average energy for each surface-peptide-water system was discarded. \bar{E}_{Ads} and the uncertainty ΔE_{Ads} was then obtained

from multiple independent simulations of the same system with different initial conformations using block averages over two simulations of $E_{Surf + P+H_2O}$ of lowest average energies $E_{Ads,2}$, over three simulations of $E_{Surf + P+H_2O}$ of lowest average energies $E_{Ads,3}$, and over four simulations of $E_{Surf + P+H_2O}$ of lowest average energies $E_{Ads,4}$:

$$\bar{E}_{Ads} = (E_{Ads,2} + E_{Ads,3} + E_{Ads,4}) / 3 \quad (2)$$

$$\Delta E_{Ads} =$$

$$\pm (|E_{Ads,4} - E_{Ads,3}| + |E_{Ads,4} - E_{Ads,2}| + |E_{Ads,3} - E_{Ads,2}|) / 3 \quad (3)$$

These block averages reasonably represent the Boltzmann averages and overall uncertainties ΔE_{Ads} were typically <10% of \bar{E}_{Ads} (Figure 4).

The overall reliability of computed adsorption energies is between 10 and 20%. In addition to the statistical uncertainty according to Equation (3), possible limitations of the method include the nature and accuracy of the force field, neglect of electronic structure, neglect of polarization at the interfaces, as well as limitations in simulation time. The force field is likely a limited source of error due to the absence of significant covalent peptide bonding to metal surfaces in aqueous solution.^[36,38,41,44] Polarization is a minor effect due to strong epitaxial interactions on {111} surfaces and similar polarity of water and peptides.^[50] As mentioned, full relaxation of the peptide backbone can be a challenge on strongly attractive surfaces, however, the small uncertainty in ΔE_{Ads} , visual inspection, and Ramachandran analysis indicate good convergence in conformation sampling.

Supporting Information

Supporting Information is available from the Wiley Online Library or from the author.

Acknowledgements

We are grateful for support by the Air Force Research Laboratory, Wright-Patterson Air Force Base, Ohio, the National Science Foundation (DMR-0955071), and the University of Akron. MS acknowledges support by NSF-MRSEC at the University of Washington. We also acknowledge the Ohio Supercomputing Center for the generous allocation of computer resources.

- [1] C. M. Niemeyer, *Angew. Chem. Int. Ed.* **2001**, *40*, 4128.
- [2] J. C. Smith, K.-B. Lee, Q. Wang, M. G. Finn, J. E. Johnson, M. Mrksich, C. A. Mirkin, *Nano Lett.* **2003**, *3*, 883.
- [3] J. Chen, B. J. Wiley, Y. Xia, *Langmuir* **2007**, *23*, 4120.
- [4] C.-C. You, A. Chompoosor, V. M. Rotello, *Nano Today* **2007**, *2*, 34.
- [5] Z. H. Nie, D. Fava, E. Kumacheva, S. Zou, G. C. Walker, M. Rubinstein, *Nat. Mater.* **2007**, *6*, 609.

- [6] W. Jiang, B. Y. S. Kim, J. T. Rutka, W. C. W. Chan, *Nat. Nanotechnol.* **2008**, *3*, 145.
- [7] M. B. Dickerson, K. H. Sandhage, R. R. Naik, *Chem. Rev.* **2008**, *108*, 4935.
- [8] S. Lal, S. E. Clare, N. J. Halas, *Acc. Chem. Res.* **2008**, *41*, 1842.
- [9] S. H. D. Lacerda, J. J. Park, C. Meuse, D. Pristinski, M. L. Becker, A. Karim, J. F. Douglas, *ACS Nano* **2010**, *4*, 365.
- [10] R. Coppage, J. M. Slocik, B. D. Briggs, A. I. Frenkel, H. Heinz, R. R. Naik, M. R. Knecht, *J. Am. Chem. Soc.* **2011**, *133*, 12346.
- [11] C. Y. Chiu, Y. J. Li, L. Y. Ruan, X. C. Ye, C. B. Murray, Y. Huang, *Nat. Chem.* **2011**, *3*, 393.
- [12] R. Braun, M. Sarikaya, K. Schulten, *J. Biomater. Sci. Polym. Edn.* **2002**, *13*, 747.
- [13] R. Djalali, Y. F. Chen, H. Matsui, *J. Am. Chem. Soc.* **2003**, *125*, 5873.
- [14] X. Y. Fu, Y. Wang, L. X. Huang, Y. L. Sha, L. L. Gui, L. H. Lai, Y. Q. Tang, *Adv. Mater.* **2003**, *15*, 902.
- [15] Y. Shao, Y. Jin, S. Dong, *Chem. Commun.* **2004**, 1104.
- [16] R. R. Naik, S. E. Jones, C. J. Murray, J. C. McAuliffe, R. A. Vaia, M. O. Stone, *Adv. Funct. Mat.* **2004**, *14*, 25.
- [17] J. M. Slocik, M. O. Stone, R. R. Naik, *Small* **2005**, *1*, 1048.
- [18] L. L. Atanasoska, J. C. Buchholz, G. A. Somorjai, *Surface Sci.* **1978**, *72*, 189.
- [19] O. Carny, D. E. Shalev, E. Gazit, *Nano Lett.* **2006**, *6*, 1594.
- [20] N. L. Rosi, D. A. Giljohann, C. S. Thaxton, A. K. R. Lytton-Jean, M. S. Han, C. A. Mirkin, *Science* **2006**, *312*, 1027.
- [21] J. M. Slocik, R. R. Naik, *Adv. Mater.* **2006**, *18*, 1988.
- [22] D. L. Feldheim, B. E. Eaton, *ACS Nano* **2007**, *1*, 154.
- [23] E. Kharlampieva, J. M. Slocik, T. Tsukruk, R. R. Naik, V. V. Tsukruk, *Chem. Mater.* **2008**, *20*, 5822.
- [24] J. E. Millstone, W. Wei, M. R. Jones, H. J. Yoo, C. A. Mirkin, *Nano Lett.* **2008**, *8*, 2526.
- [25] S. K. Kang, I. Choi, J. Lee, Y. Kim, J. Yi, *Curr. Appl. Phys.* **2008**, *8*, 810.
- [26] Z. J. Wang, J. H. Yuan, M. Zhou, L. Niu, A. Ivaska, *Appl. Surf. Sci.* **2008**, *254*, 6289.
- [27] K. T. Nam, Y. J. Lee, E. M. Krauland, S. T. Kottmann, A. M. Belcher, *ACS Nano* **2008**, *2*, 1480.
- [28] M. Hnilova, E. E. Oren, U. O. S. Seker, B. R. Wilson, S. Collino, J. S. Evans, C. Tamerler, M. Sarikaya, *Langmuir* **2008**, *24*, 12440.
- [29] C. Chen, P. Zhang, N. L. Rosi, *J. Am. Chem. Soc.* **2008**, *130*, 13555.
- [30] C. R. So, J. L. Kulp III, E. E. Oren, H. Zareie, C. Tamerler, J. S. Evans, M. Sarikaya, *ACS Nano* **2009**, *3*, 1525.
- [31] Z. P. Liu, P. Hu, A. Alavi, *J. Am. Chem. Soc.* **2002**, *124*, 14770.
- [32] A. Bilic, J. R. Reimers, N. S. Hush, J. Hafner, *J. Chem. Phys.* **2002**, *116*, 8981.
- [33] A. Michaelides, V. A. Ranea, P. L. de Andres, D. A. King, *Phys. Rev. Lett.* **2003**, *90*, 216102.
- [34] M. M. Seibert, A. Patriksson, B. Hess, D. van der Spoel, *J. Mol. Biol.* **2005**, *354*, 173.
- [35] N. Kantarci, C. Tamerler, M. Sarikaya, T. Haliloglu, P. Doruker, *Polymer* **2005**, *46*, 4307.
- [36] P. Schravendijk, N. van der Vegt, L. Delle Site, K. Kremer, *ChemPhysChem* **2005**, *6*, 1866.
- [37] A. Ferretti, C. Baldacchini, A. Calzolari, R. Di Felice, A. Ruini, E. Molinari, M. G. Betti, *Phys. Rev. Lett.* **2007**, *99*, 046802.
- [38] P. Schravendijk, L. M. Ghiringhelli, L. Delle Site, N. F. A. van der Vegt, *J. Phys. Chem. C* **2007**, *111*, 2631.
- [39] L. M. Ghiringhelli, L. Delle Site, *J. Am. Chem. Soc.* **2008**, *130*, 2634.
- [40] G. Hong, H. Heinz, R. R. Naik, B. L. Farmer, R. Pachter, *ACS Appl. Mater. Interfaces* **2009**, *1*, 388.
- [41] F. Mehmood, A. Kara, T. S. Rahman, C. R. Henry, *Phys. Rev. B* **2009**, *79*, 075422.
- [42] R. B. Pandey, H. Heinz, J. Feng, B. L. Farmer, J. M. Slocik, L. R. Drummy, R. R. Naik, *Phys. Chem. Chem. Phys.* **2009**, *11*, 1989.
- [43] A. V. Verde, J. M. Acres, J. K. Maranas, *Biomacromolecules* **2009**, *10*, 2118.
- [44] H. Heinz, B. L. Farmer, R. B. Pandey, J. M. Slocik, S. S. Patnaik, R. Pachter, R. R. Naik, *J. Am. Chem. Soc.* **2009**, *131*, 9704.
- [45] H. Heinz, *J. Comp. Chem.* **2010**, *31*, 1564.
- [46] A. Calzolari, G. Cicero, C. Cavazzoni, R. Di Felice, A. Catellani, S. Corni, *J. Am. Chem. Soc.* **2010**, *132*, 4790.
- [47] R. B. Pandey, H. Heinz, J. Feng, B. L. Farmer, *J. Chem. Phys.* **2010**, *133*, 095102.
- [48] J. A. Keith, D. Fantauzzi, T. Jacob, A. C. T. van Duin, *Phys. Rev. B* **2010**, *81*, 235404.
- [49] M. Hoefling, F. Iori, S. Corni, K. E. Gottschalk, *Langmuir* **2010**, *26*, 8347.
- [50] H. Heinz, K. C. Jha, J. Luettmer-Strathmann, B. L. Farmer, R. R. Naik, *J. R. Soc. Interface* **2011**, *8*, 220.
- [51] J. Feng, R. B. Pandey, R. J. Berry, J. M. Slocik, R. R. Naik, B. L. Farmer, H. Heinz, *Soft Matter* **2011**, *7*, 2113.
- [52] J. Bardeen, *Phys. Rev.* **1940**, *58*, 727.
- [53] N. D. Lang, W. Kohn, *Phys. Rev. B* **1973**, *7*, 3541.
- [54] A. D. MacKerell, D. Bashford, M. Bellott, R. L. Dunbrack, J. D. Evanseck, M. J. Field, S. Fischer, J. Gao, H. Guo, S. Ha, D. Joseph-McCarthy, L. Kuchnir, K. Kuczera, F. T. K. Lau, C. Mattos, S. Michnick, T. Ngo, D. T. Nguyen, B. Prodhom, W. E. Reiher, B. Roux, M. Schlenkrich, J. C. Smith, R. Stote, J. Straub, M. Watanabe, J. Wiorkiewicz-Kuczera, D. Yin, M. Karplus, *J. Phys. Chem. B* **1998**, *102*, 3586.
- [55] H. Heinz, R. A. Vaia, B. L. Farmer, R. R. Naik, *J. Phys. Chem. C* **2008**, *112*, 17281.
- [56] T. Jarvi, A. Kuronen, M. Hakala, K. Nordlund, A. C. T. van Duin, W. A. Goddard, T. Jacob, *Eur. Phys. J. B* **2008**, *66*, 75.
- [57] T. P. Hopp, K. S. Prickett, V. L. Price, R. T. Libby, C. J. March, D. P. Cerretti, D. L. Urdal, P. J. Conlon, *Nat. Biotechnol.* **1988**, *6*, 1204.
- [58] On the even surface (Figure 3a), the distance of the probe atom was 3 Å from the top layer of Au atoms. On the stepped surface (Figure 3b), the distance of the probe atom was 3 Å from the top layer of Au atoms and increased to 4 Å at the outer edge. The surface potential at 3 Å distance in this region is thus slightly lower (further below zero) than the displayed value. On the spherical surface (Figure 3c), the surface potential corresponds to a sphere of 13 Å radius from the center atom of the nanoparticle. The distance normal to nearest Au atoms ranges from 3.01 Å to 4.84 Å so that the surface potential at 3 Å distance in some regions is somewhat lower (further below zero) than displayed.
- [59] H. J. Ryu, L. Sanchez, H. A. Keul, A. Raj, M. R. Bockstaller, *Angew. Chem. Int. Ed.* **2008**, *120*, 7751.
- [60] M. A. van Hove, R. J. Koestner, P. C. Stair, J. P. Biberian, L. L. Kesmodel, I. Bartos, G. A. Somorjai, *Surf. Sci.* **1981**, *103*, 189.
- [61] U. Harten, A. M. Lahee, J. P. Toennies, C. Woll, *Phys. Rev. Lett.* **1985**, *54*, 2619.
- [62] T. M. Trimble, R. C. Cammarata, K. Sieradzki, *Surf. Sci.* **2003**, *531*, 8.
- [63] HyperChem 7.5; Hypercube Inc.: Gainesville, FL, **2006**.
- [64] Materials Studio and Discover program. Version 96.0/4.0.0; Accelrys, Inc.: San Diego, CA, **2005**.
- [65] H. Heinz, U. W. Suter, *J. Phys. Chem. B* **2004**, *108*, 18341.
- [66] H. Heinz, H. Koerner, K. L. Anderson, R. A. Vaia, B. L. Farmer, *Chem. Mater.* **2005**, *17*, 5658.
- [67] H. Heinz, R. A. Vaia, B. L. Farmer, *J. Chem. Phys.* **2006**, *124*, 224713.
- [68] H. Heinz, W. Paul, U. W. Suter, K. Binder, *J. Chem. Phys.* **2004**, *120*, 3847.

- [69] H. Heinz, R. A. Vaia, H. Koerner, B. L. Farmer, *Chem. Mater.* **2008**, *20*, 6444.
- [70] Y. T. Fu, H. Heinz, *Chem. Mater.* **2010**, *22*, 1595.
- [71] P. Dauber-Osguthorpe, V. A. Roberts, D. J. Osguthorpe, J. Wolff, M. Genest, A. T. Hagler, *Proteins: Struct. Funct. Genetics* **1988**, *4*, 31.
- [72] J. C. Phillips, R. Braun, W. Wang, J. Gumbart, E. Tajkhorshid, E. Villa, C. Chipot, R. D. Skeel, L. Kale, K. Schulten, *J. Comput. Chem.* **2005**, *26*, 1781.
- [73] S. J. Plimpton, *J. Comput. Phys.* **1995**, *117*, 1.

Received: September 30, 2011

Published online: February 10, 2012